RSC Advances

PAPER

View Article Online
View Journal | View Issue

Cite this: *RSC Adv.*, 2024, **14**, 29242

Evaluation of magnetic hyperthermia, drug delivery and biocompatibility (bone cell adhesion and zebrafish assays) of trace element co-doped hydroxyapatite combined with Mn–Zn ferrite for bone tissue applications

Tanatsaparn Tithito,[a] Siwapech Sillapaprayoon,[b] Varissara Chantho,[b] Wittaya Pimtong,[b] Jirawan Thongbunchoo,[cd] Narattaphol Charoenphandhu,[cdef] Nateetip Krishnamra,[cd] Nararat Yong,[b] Aurachat Lert-itthiporn,[b] Weerakanya Maneeprakorn *[b] and Weeraphat Pon-On *[a]

The treatment and regeneration of bone defects, especially tumor-induced defects, is an issue in clinical practice and remains a major challenge for bone substitute material invention. In this research, a composite material of biomimetic bone-like apatite based on trace element co-doped apatite ($Ca_{10-\delta}M_{\delta}(PO_4)_{5.5}(CO_3)_{0.5}(OH)_2$; M = trace elements of Mg, Fe, Zn, Mn, Cu, Ni, Mo, Sr and BO_3^{3-}; THA)-integrated-biocompatible magnetic Mn–Zn ferrite ((Mn, Zn)Fe_2O_4 nanoparticles, BioMags) called THAiBioMags was prepared *via* a co-precipitation method. Its characteristics, *i.e.*, physical properties, hyperthermia performance, ion/drug delivery, were investigated *in vitro* using osteoblasts (bone-forming cells) and *in vivo* using zebrafish. The synthesized THAiBioMags particles revealed superparamagnetic behaviour at room temperature. Under the influence of an alternating magnetic field, THAiBioMags particles demonstrated a change in temperature, indicating their potential for magnetic hyperthermia, in which THAiBioMags further exhibited a specific absorption rate (SAR) value of 9.44 W g^{-1} (I = 44 A, H = 6.03 kA m^{-1} and f = 130 kHz). In addition, the as-prepared particles demonstrated sustained ion/drug (doxorubicin (DOX)) release under physiological pH conditions. Biological assay analysis revealed that THAiBioMags exhibited no toxicity towards osteoblast cells and demonstrated excellent cell adhesion properties. *In vivo* studies employing an embryonic zebrafish model showed the non-toxic nature of the synthesized THAiBioMags particles, as revealed by evaluation of the survivability, hatching rate, and embryonic morphology. These results could potentially lead to the design and fabrication of magnetic scaffolds to be used in therapeutic treatment and bone regeneration.

Received 25th May 2024
Accepted 18th August 2024

DOI: 10.1039/d4ra03867c

rsc.li/rsc-advances

1 Introduction

A biomaterial with dual functional properties that could be applied in therapeutics and for bone regeneration is the gold standard for the treatment of bone diseases, especially bone cancer.[1–3] During the past few decades, biomagnetic scaffolds comprising calcium phosphate-based bioceramics combined with magnetic materials have gained extensive recognition and application in the field of bone therapy and regeneration.[4–13] Calcium phosphate-based bioceramics are biocompatible and known for their ability to improve osteoconductivity. Meanwhile, the inclusion of a magnetic element has been shown to result in magnetic hyperthermia capable of killing tumor cells when exposed to an external magnetic field (EMF). A number of investigations on magnetic calcium phosphate for bone tissue engineering have been reported. Yang Xia *et al.*[6] demonstrated the potential of magnetic calcium phosphate combined with superparamagnetic iron oxide nanoparticles (IONPs) as bioactive magnetic scaffolds in bone tissue engineering. In the presence of a magnetic field (MF), this material exhibited synergistic effects that enhanced the osteogenic differentiation

[a]*Department of Physics, Faculty of Science, Kasetsart University, Bangkok, 10900, Thailand. E-mail: fsciwpp@ku.ac.th*

[b]*National Nanotechnology Center (NANOTEC), National Science and Technology Development Agency (NSTDA), Pathum Thani 12120, Thailand. E-mail: weerakanya@nanotec.or.th*

[c]*Center of Calcium and Bone Research (COCAB), Faculty of Science, Mahidol University, Bangkok, 10400, Thailand*

[d]*Department of Physiology, Faculty of Science, Mahidol University, Bangkok, 10400, Thailand*

[e]*Institute of Molecular Biosciences, Mahidol University, Nakhon Pathom, 73170, Thailand*

[f]*The Academy of Science, The Royal Society of Thailand, Dusit, Bangkok, 10300, Thailand*

of seeded stem cells and bone tissue formation. Juan A. Ramos-Guivar *et al.*[7] studied the structural, morphological, heat release and biological properties of hydroxyapatite functionalized γ-Fe_2O_3 nanoparticles. They showed that the studied materials exhibited excellent biocompatibility with no observable toxicity and thus could potentially be used in magnetic hyperthermia therapy for cancer and bone regeneration. Krzysztof Marycz *et al.*[9] prepared nanocomposites of $Ca_5(PO_4)_3OH/Fe_3O_4$ (called nHAp/IO), which were functionalized with microRNAs (nHAp/IO@miR-21/124). They demonstrated its ability to promote the survival and metabolism of bone cells and enhance the functional differentiation of pre-osteoblasts MC3T3-E1 in co-cultures with pre-osteoclasts. Sudip Mondal *et al.*[10] prepared hydroxyapatite coated iron oxide (IO-HA), which demonstrated a remarkably high efficiency in eliminating nearly all the experimental MG-63 osteosarcoma cells. This research opens new avenues for biomaterial applications in anticancer therapies based on magnetic hyperthermia.

Up to now, studies on magnetic scaffolds based on bioactive glass have been mostly investigated for their ability to induce both hyperthermia and bone regeneration.[14–22] The magnetic nanomaterials embedded in the bioactive glass ceramics provided a promising approach for therapeutic treatments *via* successive hyperthermia upon EMF stimulation. Meanwhile, bioactive glasses could stimulate the formation of a bone-like matrix *via* the release of bioactive ions, such as calcium ion (Ca^{2+}), silicate ions (SiO_3^{2-}), phosphate ion (PO_3^{2-}), zinc ion (Zn^{2+}), magnesium ion (Mg^{2+}), strontium ion (Sr^{2+}), iron ion (Fe^{2+}), cobalt ion (Co^{2+}), or copper ion (Cu^{2+}). Zilin Zhang *et al.*[19] synthesized a magnetic bioactive glass-ceramic (MBGC) of magnetic Fe_3O_4/bioactive glass-ceramic ($CaO–SiO_2–P_2O_5–MgO$) scaffolds with the appropriate bioactivity and ability to induce hyperthermia. This novel magnetic glass-ceramic scaffold appeared to be a promising biomaterial to be used for bone repair after tumor resection. On the other hand, Cansu Taşar *et al.*[20] synthesized a bioactive glass combined with superparamagnetic iron oxide nanoparticles (SPIONs), which promoted bone cell viability independent of generating a magnetic field. Most recently, Jiafei Gu *et al.*[21] used the sol–gel method to prepare multifunctional phosphate glasses in the system of $50P_2O_5–40CaO–(10-x)Na_2O–xFe_2O_3/CuO$ ($x = 0$, 2, 5, 8 mol%), which induced hyperthermia to effectively kill tumor cells. In addition, the glasses degraded over time and released P, Ca, Na and Fe, promoting bone cell proliferation and osteogenic differentiation.

Based on the developmental concept of biomaterials possessing dual functional properties for bone therapy and regeneration, a multifunctional composite scaffold (controlled ion/drug release, magnetic heating capabilities, as a scaffold for bone cell adhesion) was developed in this study. As a proof of concept, the composite involved the successive co-doping of multiple trace elements (Mg, Fe, Zn, Mn, Cu, Ni, Mo, Sr, Co, BO_3^{3-} and CO_3^{2-}) into the hydroxyapatite (HAp) [$(Ca_{10-\delta}M_\delta(PO_4)_{5.5}(CO_3)_{0.5}(OH)_2$), M = trace elements (THA)] integrated-biocompatible magnetic Mn–Zn ferrite [(Mn, Zn)Fe_2O_4] nanoferrite particles (BioMags) (THAiBioMags), resulting in a magnetic composite material for bone treatment and bone regeneration. Previous studies reported that the presence of ions in calcium phosphate composite played an essential part in the exertion of biological action, such as the stimulation of osteogenesis, angiogenesis, anti-bacterial activities, as well as in their mechanical properties.[23–26] Meanwhile, (Mn, Zn)Fe_2O_4 could effectively enhance heat generation in the range of 41–46 °C (a promising strategy for hyperthermia treatment) when stimulated by an EMF.[27–30] Furthermore, manganese–zinc ferrite had considerable potential due to its non-toxicity and responsiveness to magnetic fields. Thus, the constructed multifunctional THAiBioMags provide a unique biomaterial scaffold for bone tumor treatment with combined therapeutic and bone tissue regenerative properties. Herein, we revealed that THAiBioMags possessed ion/drug and heat release properties. Thus, THAiBioMags provide a promising therapeutic approach for bone tumor treatment, as well as the ability to enhance osteoblast–osteoclast coupling.

2 Experiment

2.1 Chemical reagents

Ferric chloride ($FeCl_3$ anhydrous, 99.0%), manganese nitrate ($Mn(NO_3)\cdot 4H_2O$, 97.0%) and zinc nitrate ($(Zn(NO_3))_2\cdot 6H_2O$, 98%) were obtained from UNIVAR (Australia). The chemicals used for multi-trace element co-doped hydroxyapatite (HAp) include the following: $Ca(NO_3)_2\cdot 4H_2O$ (calcium nitrate, 99.0%) (Sigma, USA), $(NH_4)_2HPO_4$ (diammonium hydrogen phosphate, 99.0%) (Kemaus, Australia), Na_2CO_3 (sodium carbonate, 99.8%) (Rankem, India), $MgCl_2\cdot 6H_2O$ (magnesium chloride, 99.0%) (Fluka Chemika, Switzerland), H_3BO_3 (boric acid, 99.5%) (Merck, Germany), $ZnCl_2$ (zinc chloride, 98.0%) (Sigma-Aldrich, USA), $CuCl_2\cdot 2H_2O$ (copper(II) chloride dihydrate, 99.0%) (QRëC, New Zealand), $Mn(NO_3)_2\cdot 4H_2O$ (manganese(II) nitrate tetrahydrate, 97.0%) (Chem-supply, Australia), $NiCl_2\cdot 6H_2O$ (nickel(II) chloride hexahydrate, 99.9%) (Merck, Germany), $Na_2MoO_4\cdot 2H_2O$ (sodium molybdate dihydrate, 99.5%) (Kemaus, Australia), $SrCl_2\cdot 6H_2O$ (strontium chloride hexahydrate, 99.0%) (Univa, New Zealand) and $CoCl_2\cdot 6H_2O$ (cobalt chloride hexahydrate, 98.0%) (Sigma-Aldrich, USA), NH_4OH (ammonium solution, 28.0%) (QRëC, New Zealand). Doxorubicin (DOX) (Fluka, Biochemika) was used as the model anticancer drug. All chemicals were of analytical grade, and were used without further purification.

2.2 Synthesis of (Mn, Zn)Fe_3O_4 (MZF) nanoparticles

Magnetic nanoferrite particles of (Mn, Zn)Fe_2O_4 were done using an alkaline co-precipitation method, as described in a previous report.[31] Briefly, the nitrate salt of $Mn(NO_3)\cdot 4H_2O$ (0.9 mmol), $Zn(NO_3)_2\cdot 6H_2O$ (0.1 mmol) and anhydrous $FeCl_3$ (2 mmol) were mixed in 50 mL of deionized water, along with 10 mL of ethylene glycol (EG) and 5 mL of 0.2 M HCl, under vigorous stirring. The solution was stirred for an additional 30 minutes at room temperature. Then, the mixed salt solution was added dropwise into a 250 mL round-bottom flask containing 3 g of NaOH and 0.54 g of SDS, which were dissolved in 25 mL of distilled water at 80 °C with magnetic stirring for 30

minutes. At the end of the reaction, the resulting black nanoferrite particles of (Mn, Zn)Fe_2O_4 were magnetically collected from the solution, washed three times with ethanol and deionized water to obtain a neutral pH, and dried at 80 °C for 12 h. To activate the carboxyl groups on the (Mn, Zn)Fe_2O_4 nanoparticles, a pre-dissolved citric acid solution (0.05 M) was added to the magnetic particles, resulting in the formation of carboxylic functional (Mn, Zn)Fe_2O_4 (MZF). The nanoparticles were obtained through freeze-drying.

2.3 Synthesis of multi-trace elements (THA)-integrated (Mn, Zn)Fe_3O_4 (THAiBioMags) composites

The THAiBioMags composite particles were synthesized by wet chemical precipitation technique. Briefly, 1 g of synthesized magnetic (Mn, Zn)Fe_3O_4 nanoparticles was dispersed in an anion solution consisting of $(NH_4)_2HPO_4$ (230 mM), H_3BO_3 (0.01 mM) and Na_2CO_3 (8 mM) in 250 mL of deionized water, containing appropriate amounts of P with BO_3^{3-} and CO_3^{2-}, respectively. Separated cation solutions were prepared using $Ca(NO_3)_2 \cdot 4H_2O$ (380 nM), $MgCl_2 \cdot 6H_2O$ (0.50 mM), $FeCl_2 \cdot 4H_2O$ (0.075 mM), $ZnCl_2$ (0.08 mM), $Mn(NO_3)_2 \cdot 4H_2O$ (0.006 mM), $CuCl_2 \cdot 2H_2O$ (0.02 mM), $NiCl_2 \cdot 6H_2O$ (0.001 nM), $Na_2MoO_4 \cdot 2H_2O$ (0.001 mM), $CoCl_2 \cdot 6H_2O$ (0.001 mM), and $SrCl_2 \cdot 6H_2O$ (0.008 mM) as sources for Ca, Mg, Fe, Zn, Mn, Cu, Ni, Mo, Co, and Sr, respectively. These chemicals were mixed in 250 mL of deionized water in a beaker, while being stirred with a magnetic stirrer. In the typical synthesizing THAiBioMags process, the cation and anion solutions containing magnetic (Mn, Zn)Fe_3O_4 nanoparticles were mixed together by dropping the cation solution into the anion solution. The pH of this mixture was maintained at 9 by adding $(NH_4)OH$ dropwise, and this process was carried out under constant stirring. After several minutes, multi-trace elements (THA)-integrated (Mn, Zn)Fe_3O_4 (THAiBioMags) began to coprecipitate. The powders were then separated from the supernatant solutions by filtered, and washed with de-ionized water until the pH reached approximately 7. The samples were then freeze-dried and heated to 500 °C for 2 hours under an ambient air atmosphere.

2.4 Doxorubicin (DOX) drug loading and release

DOX-loaded THAiBioMags particles were synthesized as follows: 1 mL of DOX solution (1 mg mL^{-1}, as the drug model) was added to 5 mL of THAiBioMags solution (10 mg mL^{-1} in PBS at pH of 7.4), and mixed with a magnetic stirrer for 4 h under dark condition. At the end of the reaction, the DOX-loaded THAiBioMags particles were detached from the solution magnetically using an NdFeB magnet. Subsequently, the resulting particles were freeze-dried. For the *in vitro* drug release study, DOX-THAiBioMags particles were immersed in 15 mL PBS buffer solution (5 mg mL^{-1}) (pH 7.4) under constant stirring at a rate of 100 rpm for more than a day at 37 °C. At the end of each incubation period (the different incubation periods used were 0.5, 1, 2, 3, 4, 5, 6, 7, 8, 9, 10, 15, 20, 25 and 30 h), 3 mL of the released supernatant medium was withdrawn and replenished with 3 mL of fresh buffer solution. Then, the amounts of DOX released into the buffer solution were determined by measuring their absorbance with a UV-visible spectrophotometer (Jenway, model 6405) at a wavelength of 480 nm. The percentage of drug released from the particles was calculated by the following equation:

$$\%\ \text{Release} = \frac{\text{amount of drug in release medium at time } t}{\text{amount of drug loaded in particle}} \times 100 \quad (1)$$

The drug content in the supernatant was determined by comparing the measured absorbance to the standard curve for the DOX adsorption, represented by the following equation: $C_i = 0.1042A_i + 0.00018$; $R^2 = 0.9907$, where C_i was the DOX drug concentration (0.002 to 0.01 mg mL^{-1}) and A_i was the UV-vis absorbance at a wavelength of 480 nm. The DOX release experiments were performed in triplicate, and the amount of DOX released at each time point was determined as a mean value ± standard derivation (SD). To understand the processes associated with DOX release from the THAiBioMags particles, the Korsmeyer–Peppas, Higuchi and Weibull model[32–34] was used to fit the DOX release kinetic profiles.

2.5 Characterization of the THAiBioMags composite

2.5.1 Physico-chemical characterizations. The surface morphology and element composition of the as-prepared THAiBioMags particles were characterized using a scanning electron microscope (SEM) and an energy dispersion spectroscopy (EDS) (FEI SEM Quanta 450, Brno, Czech). The spectroscopic characterizations were performed using attenuated total reflectance-Fourier transform infrared spectroscopy (ATR-FTIR) at 4 cm^{-1} resolution with 32 scans in the frequency range of 400–4000 cm^{-1}. To determine the presence of the different phases of the synthesized particles, an X-ray diffractometer (XRD) (D8 Advance Bruker, Karlsruhe, Germany) was used to determine the crystal structure of the THAiBioMags powder using Cu Kα radiation ($\lambda = 0.15405$ nm). The magnetic properties of the THAiBioMags particle were measured at room temperature using a vibrating sample magnetometer (VSM) (Lakeshore, Model 4500, Carson, CA, USA). The shape and size of the as-prepared nanoparticles at the nanoscale were examined using a transmission electron microscope (TEM) (TEM-Hitachi HI7700, Tokyo, Japan).

2.5.2 Evaluation on the heating ability. To evaluate the synthesized magnetic nanoferrite particles of the (Mn, Zn)Fe_3O_4 and THAiBioMags particles as a potential candidate for hyperthermia, the rise in temperature as a function of time was evaluated. The temperature–time profiles of the particles were recorded using a home-made alternating magnetic field (AMF) operated at 3, 5 and 7 kW. The current is passed through a 6-turn coil, 30 mm in diameter, made of copper tube. Specifically, the temperature increase in a solution containing the particles at a concentration of 1 mg mL^{-1} when exposed to AMF ($I = 44$ A and $f = 130$ kHz) for 30 minutes was recorded. The hyperthermia performance was assessed using the specific absorption rate (SAR), which was calculated based on the heating

efficiency of the nanoparticles. SAR was determined using the following formula:[35,36]

$$\text{SAR (W g}^{-1}) = [C_w/m] \times [dT/dt] \quad (2)$$

where C_w was the specific heat capacity of the medium (water) (4.186 J g^{-1} $°C^{-1}$), m was the magnetic particle concentration, and dT/dt was the rate of temperature rise obtained by fitting the heating curve to the phenomenological Box-Lucas model (eqn (2)), which was applicable for calorimetric measurements under non-diabatic condition.

$$T = T_0 + T_{max}(1 - e^{-Bt}) \quad (3)$$

where T_0 was the nonzero starting temperature, T_{max} was the maximum temperature difference in the heating curve, and B was the fitting parameter of the curve. The product ($T_{max} \times B$) was the rate.

2.5.3 Bioactivity of the THAiBioMags in SBF. The bioactivity of synthesized THAiBioMags and sHA (control) was studied in a simulated body fluid (SBF) solution prepared using the Kokubo method, according to the method reported previously,[37] in an incubator for 7 days at 37 °C. SBF is a solution with an ion concentration close to that of human blood plasma. It is made by buffering the following chemicals: NaCl (136.8 mM), $NaHCO_3$ (4.2 mM), KCl (3.0 mM), K_2HPO_4 (1.0 mM), $MgCl_2 \cdot 6H_2O$ (1.5 mM), $CaCl_2$ (2.5 mM), and Na_2SO_4 (0.5 mM) at a pH of 7.4 in $(CH_2OH)_3CNH_3$ and HCl. The bioactivity of the mineralized apatite formation of each THAiBioMags and sHA sample was assessed by immersing the pellets in 50 mL of SBF for one week at 37 °C. The SBF was replaced every three days to avoid any effects caused by changes in the cationic concentration due to the degradation of the sample. After soaking in SBF, the samples were rinsed with deionized water and dried. SEM and EDS observations were used to study the mineralized apatite and chemical elements on the surface of the samples.

2.5.4 Electrical conductivity of the ion release profile from the THAiBioMags particles. The release of trace elements from the THAiBioMags particles was studied under static conditions. Typically, 0.15 g of as-prepared sHA (synthetic hydroxyapatite, control) and THAiBioMags powders was dispersed in 15 mL distilled water at a pH of 7.4 at room temperature, and at various time points (0.5, 1, 3, 5, 7, and 14 days). At the end of each aging period, the electrical conductivity values, which were related to the number of ions released at given periods, were measured using a digital conductivity meter (HI9813-5 portable pH/EC/TDS meter, HANNA instruments, Woonsocket, RI, USA). To study the ion release profile between sHA (control) and THAiBioMags, conductivity measurements were plotted as a function of time.

2.5.5 Cell culturing and MTT assay. To evaluate the *in vitro* assay of THAiBioMags with the rat osteoblast-like UMR-106 cells, the cultivation was performed according to a method reported previously.[37] Briefly, the circular glass discs (control) and THAiBioMags discs were sterilized with 70% ethanol and placed under a UV lamp for 30 min before use. The rat osteoblast-like UMR-106 cells [American Type Culture Collection (ATCC) No. CRL-1661] grown in a Dulbecco's modified Eagle's medium (DMEM, Sigma, USA) supplemented with 10% v/v fetal bovine serum (FBS, Austria) and 100 U mL^{-1} penicillin–streptomycin (Gibco, USA) were seeded on the circular glass or THAiBioMags discs at 1×10^6 cells per well in 6-well plates. The well plates were incubated at 37 °C under humidified 5% CO_2. Then, the cell attachment and mineralization were done for 3, 5 and 7 days. To observe the cell morphology, the glass and substrates were first rinsed with phosphate buffer (pH 7.2) twice, and then fixed in 2.5% glutaraldehyde (Electron Microscopy Science, USA) in 0.1 M phosphate buffer for 3 h. Then, glass and substrate discs were dehydrated in a series of ethanol/water solution (50%, 70%, 80% and 90% v/v) and absolute ethanol, and then dried under vacuum. Cell morphology, cell adhesion and cell proliferation were visualized by SEM. Cell viability was determined using MTT (3-(4,5-dimethylthiazol-2-yl)-2,5-diphenyl-tetrazolium bromide) assay, according to the method reported previously.[37] Briefly, cells and the circular glass discs (control) and THAiBioMags discs were cultured together for 3, 5, and 7 days. Afterward, the substrate scaffolds were washed, and 20 μL of 0.5 mg mL^{-1} MTT solution was added to each sample, followed by 3.5 hours incubation. Upon removal of the MTT solution, the scaffolds were smashed, and the purple formazan crystals were dissolved in 150 μL of solvent containing 4 mM HCl and 0.1% Nondet P-40 (NP40) in isopropanol, while shaking the plate for 15 min. Then, the solution was centrifuged, and the supernatant was transferred onto another plate to measure the optical density using a micro-plate reader (Bio-Tek EL×800) at 595 nm.

2.5.6 Zebrafish maintenance and embryo collection. Adult zebrafish (*Danio rerio*) were bred and maintained at the National Nanotechnology Center (NANOTEC) using a stand-alone recirculation system (AAB-074, Yakos65, Taiwan) following standard protocols. The fish were kept under a photoperiod of 14/10 h (day/night) at 28 ± 1 °C. Embryos were obtained from natural pair-wise mating and kept in egg water (0.006% w/v sea salt in DI water). Fertilized embryos at 4 hours post-fertilization (hpf) were selected under a stereomicroscope (SZX16, Olympus, Tokyo, Japan). All study procedures have been approved by the NSTDA Institutional Animal Care and Use Committee (No. 001-2563).

2.5.7 Zebrafish embryo acute toxicity test. The zebrafish embryo acute toxicity test followed the Organization for Economic Co-operation and Development guideline number 236 (OECD 236, 2013).[38] Stock solutions of particles, including THAiBioMags, were prepared in DI water and sonicated for 10 min. For test solutions, stock solutions were serially diluted in egg water to final concentrations of 31.25, 62.5, 125, 250, and 500 μg mL^{-1}, and sonicated for 10 min. Twenty zebrafish embryos were exposed to 2 mL of each test solution in a 12-well culture plate, and 2 mL of egg water was used as a negative control. Each test solution was vortexed for 20 s before immediate addition to the well. The plates were incubated at 28.5 ± 1 °C for up to 96 h. Every 24 h, the test solutions were renewed, and dead embryos were removed. The survival, hatching, and malformation rates of zebrafish were recorded. Experiments with less than 90% survival in the control group were rejected.

At 24 and 48 hpf, the heart rates of embryos were documented by video recording using the stereomicroscope (SZX16, Olympus) equipped with the DP73 camera (Olympus).

2.6 Statistical analysis

Data were presented as the mean ± standard deviation (SD) from three independent experiments. The statistical significance between each test solution and control were determined by using one-way analysis of variance (ANOVA), followed by Tukey's test to compare the differences between groups. Statistical differences were considered significant for a p-value less than 0.05.

3 Results and discussion

The SEM micrograph and EDS analysis relating to the THAiBioMags particles are shown in Fig. 1(a and b). The micrograph in Fig. 1(a) reveals that the particles are mostly spherical with sizes of less than 100 nm. Additionally, Fig. 1(b) confirms that the particles are composed of Ca, P, Mg, Fe, Zn, Mn, Cu, Ni, Mo, Sr, Co, B and O. The XRD diffraction pattern of the as-prepared THAiBioMags particles (Fig. 1(c)) exhibits lower peak intensity and broadening of the diffraction peaks, indicating low crystallinity of THAiBioMags due to the formation of smaller crystals, making them more amorphous. The FTIR analysis of THAiBioMags is shown in (Fig. 1(d)) and presents both BioMags and THA functional groups. As a result, the characteristic bands for PO_4^{3-} appear at 479, 567, 605, 1046, and 1098 cm^{-1}. Meanwhile, the absorption bands at 3450–3575 cm^{-1} and 634 cm^{-1} are due to the stretching and vibration modes of the OH^- ions, respectively.[19] The THA functional groups in the range of 450–605 cm^{-1} have higher intensities, merging with the functional group of M–O in that region.[19] Generally, the spectra of the BioMags particles show the sharp band at 570 cm^{-1}, which corresponds to the M–O vibrations for BioMags. Additionally, three bands located at 879, 1419, and 1458 cm^{-1} can be attributed to the O–C–O stretching and bending vibration of carbonate groups.[19] This indicates the formation of carbonated apatite, a mineral phase with a composition close to that of the natural bone.

TEM images were obtained to investigate the nanosize of the obtained ions-modified hydroxyapatite and its composite with Mn–Zn nanoferrite particles ((Mn, Zn)Fe_2O_4 nanoparticles), as well as to observe how the particles interacted with each other. As shown in Fig. 2(a), the THA particles possessed a rod-like shape with an average size of approximately 25–40 nm × 7–15 nm. In contrast, the magnetic (Mn, Zn)Fe_3O_4 nanoferrite particles had a spherical-like morphology, and were in the 5–15 nanometric size range (see Fig. 2(b)). For the THAiBioMags composite particles, rod-like morphologies for THA integrating the biocompatible Mn–Zn nanoferrite were observed (see Fig. 2(c)). The magnification presented in Fig. 2(d) revealed that the (Mn, Zn)Fe_3O_4 nanoferrites (with an interplanar distance of 0.21 corresponding to a (311) plane) are well dispersed in the THA matrix, which was related to the THAiBioMags composite. Additionally, the composite particles were bigger, around 100–200 nm, than what was seen in the TEM images of THA and (Mn, Zn)Fe_3O_4 nanoferrites, which may result from the aggregation of biocompatible Mn–Zn nanoferrite (BioMags).

The magnetic properties of the prepared samples were studied by VSM. As we know, the magnetic properties of the synthetic scaffolds (magnetic scaffold) were important for dual tissue treatment and regeneration, as demonstrated by previous research.[1–3] According to Fig. 3, THA and THAiBioMags both exhibited magnetic properties, with a notable difference in their magnetic saturation (M_s) values. THA had a M_s of 0.26 emu g^{-1}, while the THAiBioMags composite showed a higher M_s of 1.62 emu g^{-1}. Notably, the magnetic saturation value of both samples decreased when compared to bare (Mn, Zn)Fe_3O_4

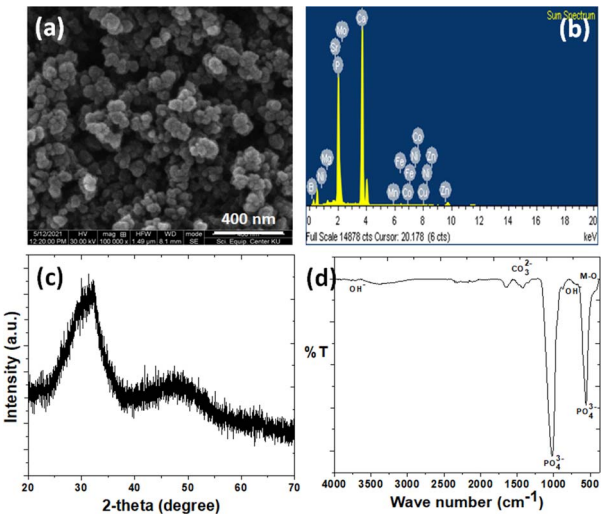

Fig. 1 Characterization of THAiBioMags particles: SEM (a), EDS (b), XRD (c) and FTIR (d).

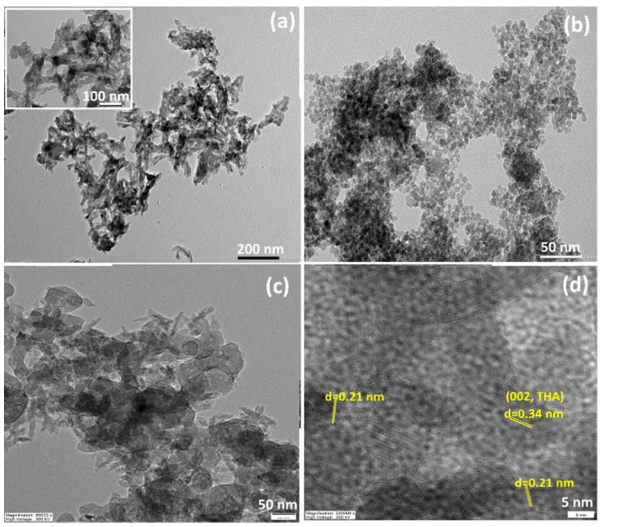

Fig. 2 TEM images of the (a) multi-trace elements co-doped apatite ($Ca_{10-\delta}M_\delta(PO_4)_{5.5}(CO_3)_{0.5}(OH)_2$, M = trace elements, THA), (b) magnetic Mn–Zn nanoferrite ((Mn, Zn)Fe_2O_4 particles, BioMags) and THAiBioMags nanoparticles at low (c) and high (d) resolution, respectively.

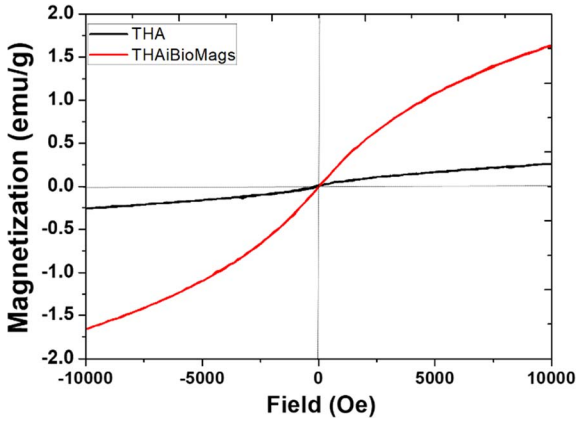

Fig. 3 Magnetic hysteresis loops of THA and THAiBioMags at room temperature.

nanoferrites (M_s = 40.53 emu g^{-1}). The lower saturation magnetization was attributed to the proximity of the non-magnetic THA compound with (Mn, Zn)Fe_3O_4, as well as the presence of less (Mn, Zn)Fe_3O_4 nanoferrites. Similar results were also reported in magnetic bioactive glass, such as the magnetic Fe_3O_4/bioactive glass-ceramic ($CaO–SiO_2–P_2O_5–MgO$) system or bioactive glass combined with superparamagnetic iron oxide nanoparticles (SPIONs).[19–21]

The heat release experiments were conducted on samples dispersed in water at concentrations of 1 mg mL^{-1} and at power levels of 3, 5, and 7 kW, as shown in Fig. 4.

It was evident that the heating properties improved with increasing power, reaching a temperature of 45 °C from 28 °C in approximately 30 minutes when using nanoparticles at an electromagnetic field frequency of 130 kHz and a current of 44 A. In this situation, the magnetic field (H) amplitude generated by the coil is calculated to be 6.03 kA m^{-1} by the following relation $H = (1.257nI/D)$, where n is the number of turn coil and

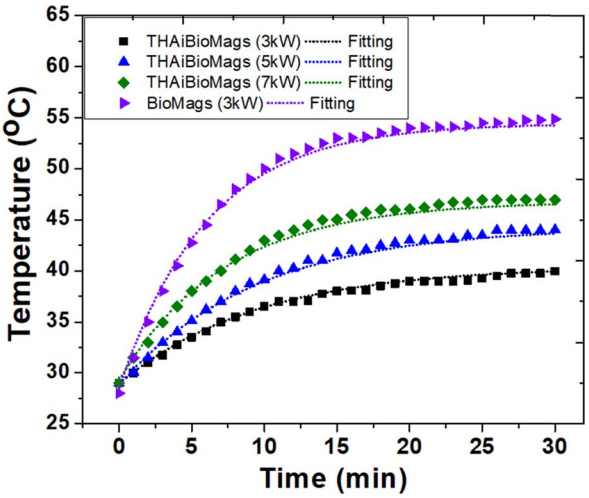

Fig. 4 Induction heating curve of magnetic Mn–Zn nanoferrite (Mn, Zn)Fe_2O_4 particles, BioMags and THAiBioMags with Box-Lucas (eqn (2)) fitting operating at 3, 5 and 7 kW with a frequency of 130 kHz.

D is the diameter (5.5 cm) of the turn. The product of the field magnetic field (H) amplitude and frequency is $Hf = (6.03 \times 10^3$ A $m^{-1}) \times (130 \times 10^3$ Hz) = 0.78×10^9 A m^{-1} s^{-1}, which was carried out within the threshold limit (Hf is taken as 5.0×10^9 A m^{-1} s^{-1}, as proposed by Hergt and Dutz[39]). The efficiency of heat conversion by magnetic nanoparticles under magnetic field stimulation was a crucial parameter for potential cancer treatment, and was estimated using the specific absorption rate (SAR), measured in W g^{-1}. The hyperthermia performance in terms of SAR was calculated from the heating efficiency of the nanoparticles, according to eqn (2) and (3). Based on the calculations using eqn (2) and (3), the SAR for THAiBioMags at power levels of 3, 5, and 7 kW were 5.25, 7.29, and 9.44 W g^{-1}, respectively. This SAR is lower compared to the (Mn, Zn)Fe_3O_4 nanoferrite, which was 18.29 W g^{-1} at a power of 3 kW. The lower SAR value of (Mn, Zn)Fe_3O_4 after composite formation may be attributed to the THA shell, which was expected to act as an insulating layer, reducing the energy transfer to the media for the (Mn, Zn)Fe_3O_4 nanoferrite. However, it was important to note that SAR depended not only on the type of materials, but also on various parameters, including the magnetic field strength, frequency, concentration, and suspension stability in aqueous media, *etc.*[40–44] As we know, heat generation and SAR loss in superparamagnetic nanoparticles under an AC magnetic field depend on both Néel's and Brownian relaxation times, denoted as τ_N and τ_B, respectively. Néel's relaxation time was approximately 10^{-9} s and involved the exponential term, $\tau_N = \tau_0 \exp\left[\frac{KV}{k_B}\right]$; $\tau_0 \approx 10^{-9}$ s, where V represented the particle volume, k_B was the Boltzmann constant, and K was a material-specific parameter. On the other hand, the Brownian relaxation time, $\tau_B = \frac{4\pi\eta r_h^3}{k_B T}$, depended on factors such as the particle size (r_h), temperature (T), and viscosity (η) of the surrounding medium.[40–42] When using THAiBioMags particles, it was important to consider that both Néel and Brownian relaxation mechanisms might impact the efficiency. Hence, using THAiBioMags particle in this situation would reduce the efficiency as both Néel and Brownian relaxation. Similar results were observed in studies involving the incorporation of superparamagnetic nanoparticles (SPIONs) into solid biomaterial matrices, such as Ca–Si-based bioactive glass.[17] For instance, in nanocomposites of superparamagnetic iron oxide nanoparticles dispersed in bioactive glass, the SAR values varied between 3–71 W g^{-1}.[17–19] Although the interdependence of SAR with magnetic field parameters such as the magnetic field frequency and amplitude made it difficult to compare the heating efficiency of the samples reported in the literature, our experimental results have clearly indicated that the SAR of our THAiBioMags composite had the potential to provide an altered magnetic scaffold for achieving controlled hyperthermia.

To investigate the mechanism and rate of drug release, two distinct behaviors were observed (Fig. 5): an initial small burst release during the first 10 hours, followed by a sustained release. The initial burst release of DOX was attributed to the

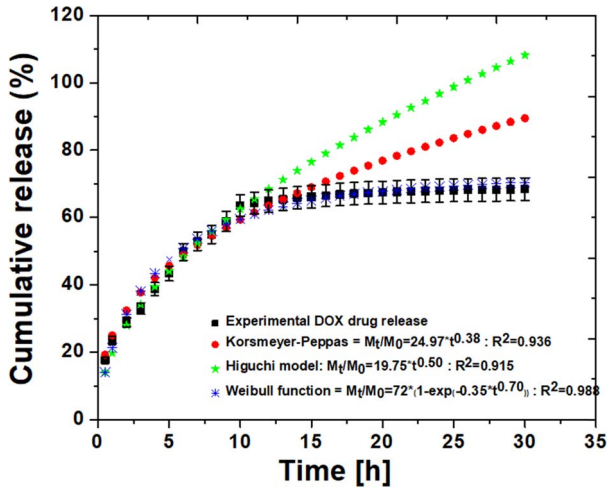

Fig. 5 The release profile of doxorubicin (DOX) and kinetic models (Korsmeyer–Peppas, Higuchi and Weibull function) applied to the release of DOX from THAiBioMags.

release of DOX molecules attached to the surface of the particles.

As observed, the overall drug release was relatively slow, with an initial burst release of approximately 64.26%, followed by a slower rate after the 10th hour. The accumulated release amount of only approximately 65.60% was released from THAiBioMags particles in the 30th hour, suggesting that the release was primarily due to the dissolution of the carrier. This is consistent with the findings from the previous reports.[45,46] To determine the possible mechanism of the DOX molecules from THAiBioMas, the well-kwon drug release kinetic models[32–34] were used to fit and predict the release mechanism. The release data were fitted based on the Korsmeyer–Peppas (KPM) ($M_t/M_0 = k_{KP}t^n$), Higuchi ($M_t/M_0 = k_H t^{0.5}$) and Weibull function ($M_t/M_0 = D_0(1 - \exp(-at^b))$). In this kinetics model, 'n' represented the release exponent, where values of $n \leq 0.45$, $n \geq 0.85$, and $0.45 < n < 0.85$ corresponded to controlled release mechanisms of the Fickian diffusion, relaxation, and non-Fickian diffusion, respectively.[32] k_{KP}, k_H, M_t and M_0 are the transport constant, release constant of Higuchi, concentration of DOX release into medium up to time t and at initial concentration, respectively.[32,33] D_0 is the diffusion coefficient, and a and b are constants.[34] A value of $b < 0.75$ suggests a Fickian diffusion release mechanism.[34] As shown in Fig. 5, during the first-10th hour, both KPM and Higuchi provided an excellent fit for the DOX release profile, but the fit was poor at longer t times. The fitting results showed the best agreement with the correlation coefficient (R^2) of 0.936 and 0.915 for the KPM and Higuchi model, respectively. Meanwhile, the KPM release exponent of "n" was 0.38, indicating that the Fickian diffusion (independent of the drug concentration) primarily governed the release of DOX from THAiBioMags at neutral levels. The Weibull function showed a better fit of the curves than the other evaluated models, showing R^2 higher than 0.988 for all curves. The obtained result with the Weibull function is $M_t/M_0 = 72(1 - \exp(-0.35t^{0.70}))$. The release index "$b = 0.70$ with <0.75" indicated that the release of DOX from the THAiBioMags particles is governed by a diffusion-based drug release.[34]

To evaluate the stability of the THAiBioMags composite scaffold, the degradation process resulted in simultaneous releases of both cations and anions, which were tracked by measuring the change in electrical conductivity of the solution. As shown in Fig. 6, the electrical conductivity of THABioMags in water was extremely low, especially over the first five hours. In contrast, the conductivity value of hydroxyapatite (sHA) increased rapidly in the first five hours and then gradually stabilized. The marked difference in the electrical conductivity curve between those of sHA and THAiBioMags could be attributed to the loss of the scaffolds, as supported by approximately 4.6% and 1.7% weight loss of sHA and THAiBioMags, respectively, after 14 days of soaking. Throughout the entire aging period, the electrical conductivity of THAiBioMags remained in the range of 0.010–0.070 mS cm^{-1}, significantly lower than that of sHA (0.020–0.273 mS cm^{-1}). The initial increase in the electrical conductivity value was likely attributed to the continuous dissolution of the scaffold, leading to the release of ionic components into the solution. However, this was a complex process involving chemical reactions and different phases of formation.

For the bioactivity assessment of the THAiBioMags and sHA (control) in SBF, the formation of apatite particles on the samples' surfaces after being soaked in SBF for 7 days was examined by SEM and EDS analysis (Fig. 7). After immersing the scaffolds in SBF for 7 days, microstructural changes on the surface of the substrates were observed. Inhomogeneous growth of apatite particles was noted on the sHA surface (Fig. 7(a and b)). As observed in Fig. 7(d and e), THAiBioMags exhibit significant surface changes, with the surface completely covered by clusters of apatite mineral particles growing as microsized crystals with nodular-like structures. These structures have diameters ranging from 2 μm to 5 μm. The Ca-to-P ratios of the particles formed on the surface, as determined

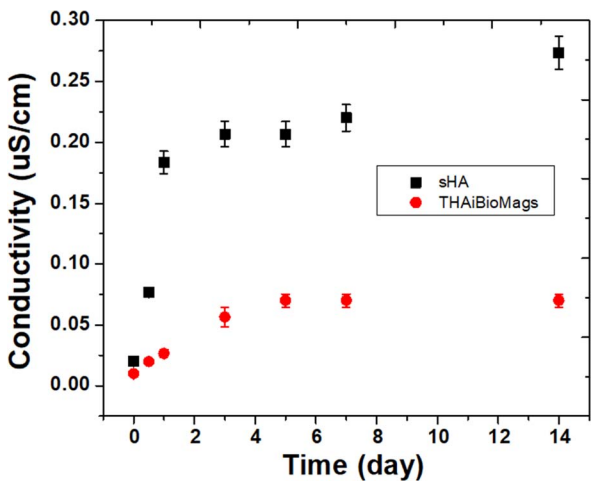

Fig. 6 The electrical conductivity of the ions released from the sHA (hydroxyapatite) and THAiBioMags.

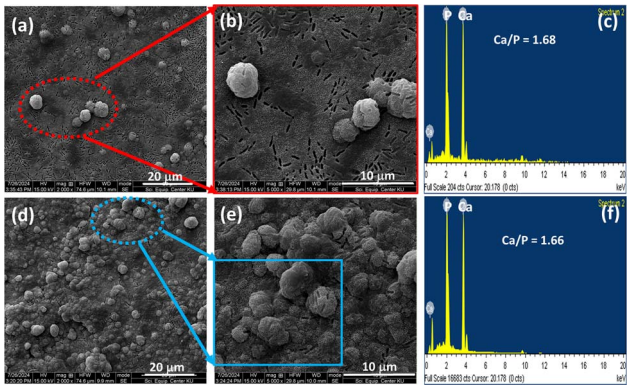

Fig. 7 SEM images of the sHA (a and b) and THAiBioMags (d and e) surfaces after immersion in SBF for 7 days. EDS analysis of particles on the surface of sHA (c) and THAiBioMags (f).

by EDS analysis, were 1.68 for sHA (Fig. 7(c)) and 1.66 for THAiBioMags (Fig. 7(f)), both close to that of natural bone (Ca/P = 1.67). The formation of mineral apatite enables the surrounding bone to come into direct contact with this layer.

To evaluate the biocompatibility of the fabricated THAiBioMags scaffolds, osteoblast-like cells were tested for their adhesion to the composite scaffolds, with a glass substrate used as a control.

As seen in Fig. 8, after 3, 5, and 7 days of culturing, the osteoblast-like cells adhered to the surface of both glass and THAiBioMags scaffolds. However, the cells on the THAiBioMags scaffold exhibited a typical spreading morphology with a polygonal appearance and more extending filopodia, indicating greater adhesion. In addition, it could be inferred that the presence of magnetic nanoferrite particles of (Mn, Zn)Fe_3O_4 and ions in the THAiBioMags scaffold did not have unfavorable influence on bone cell proliferation. The cell viability of the rat osteoblast-like cells cultured on substrates for the same culturing period was evaluated. The difference in cell viability observed by the MTT assay (Fig. 9) between the glass substrate (control) and the THAiBioMags scaffolds could be attributed to

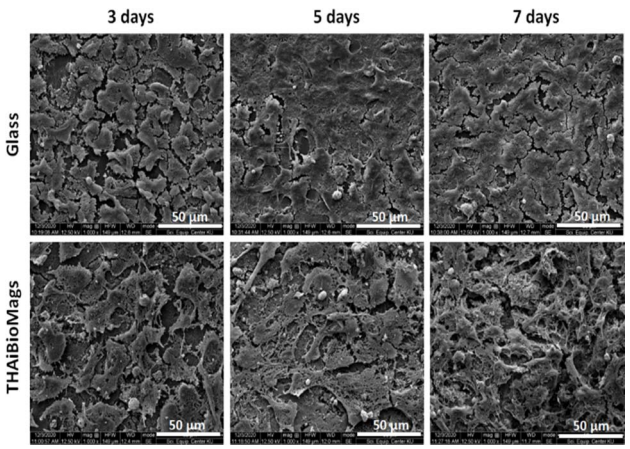

Fig. 8 Representative SEM images of osteoblast-like cells on glass and on THAiBioMags surface after 3, 5 and 7 days of culture.

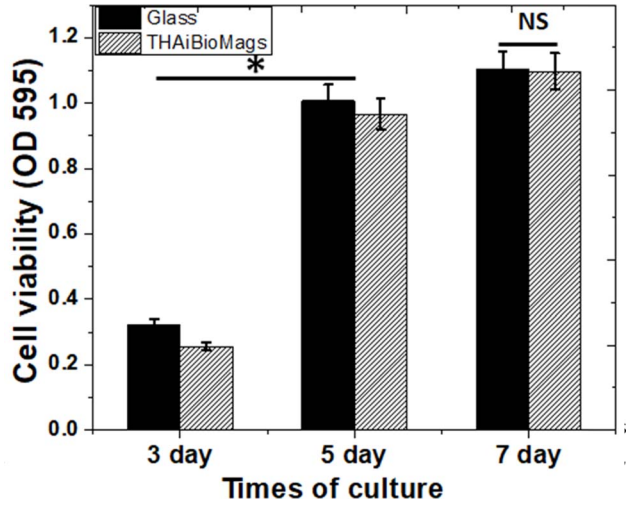

Fig. 9 MTT assay of THAiBioMags compared with the glass substrate (positive control; paired with each material) on days 3, 5, and 7. NS: no significance between the two groups, *$p < 0.05$.

variations in cell growth. However, cell viability on the surface of the THAiBioMags scaffold caught up with that of the glass scaffold from the fifth day onwards. Previous investigations have shown that the presence of certain amounts of doping elements, scaffold dissolution, and magnetic fields could promote or influence the proliferation of osteoblasts.[47–49] From these points of view, it could be attributed to the fact that the THAiBioMags scaffold in the present study appeared to allow better cell adhesion and all growth.

Zebrafish embryos have been widely used as a vertebrate model for the evaluation of nanoparticle biocompatibility.[50,51] As shown in Fig. 10, following a 96 hours exposure to sHA or THAiBioMags nanoparticles, the zebrafish embryos showed no malformation. Moreover, the survival rate (Fig. 11(a and b)), hatching rate (Fig. 11(c and d)) and heart rate (Fig. 11(e and f))

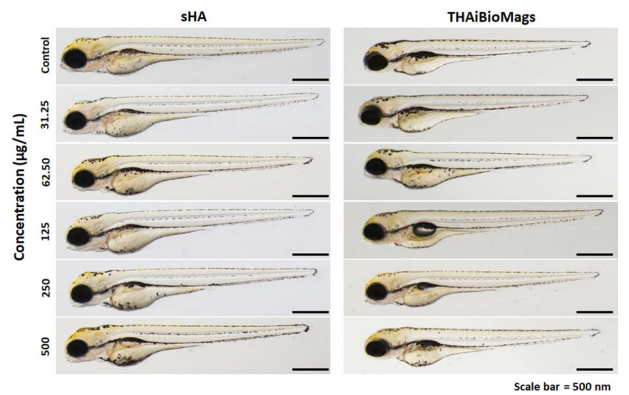

Fig. 10 Representative images of zebrafish embryos at 96 hpf after exposure to sHA and THAiBioMags.

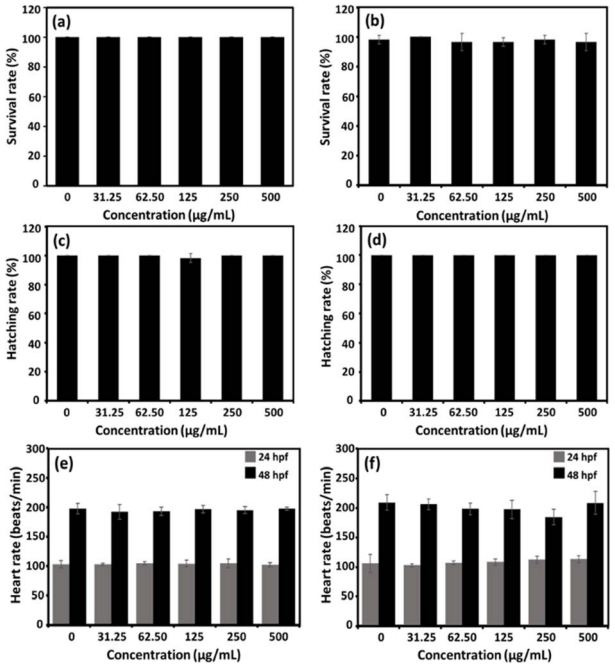

Fig. 11 Survival and hatching rates after 96 h exposure of zebrafish embryos to different concentrations of sHA (a and c) and THAiBioMags (b and d). Heart rate of zebrafish embryos at 24 and 48 hpf after exposure to different concentrations of sHA (e) and THAiBioMags (f). The data are from three independent experiments (n = 3) and presented as mean ± SD.

of the zebrafish embryos were not affected by exposure to THAiBioMags, indicating that the tested nanoparticles had no toxic effect on the developmental processes in zebrafish embryos. However, at 48 hpf, only THAiBioMags slightly reduced the embryonic heart rates at tested concentrations above 31.25 μg mL^{-1}, as shown in Fig. 11(f).

However, in a previous study, a zebrafish embryo assay was used to evaluate the toxicity and safety of bioceramics such as hydroxyapatite and bioactive glass[46–49] for use in dentistry. It was reported that different hydroxyapatite nanoparticle (HANP) morphologies (dot, long rod, sheet, and fibre)[50] at the concentration range of 0–100 mg L^{-1} could significantly impact the embryological development of zebrafish. Another study using the zebrafish model to evaluate the toxicity of dental bioceramics of mineral trioxide aggregate (MTA) and Biodentine[52] revealed a greater biocompatibility of Biodentine as compared to that of MTA. Another earlier investigation focused on the effects of the ion species and ionic dissolution products such as Cu, Sr, Mg and Si ions from bioactive glass,[51,53] and reported no toxicity or developmental abnormalities in zebrafish embryo. To the best of our knowledge, the present findings represent the first report on the non-toxicity of multi trace elements (Mg, Fe, Zn, Mn, Cu, Ni, Mo, Sr, BO_3^{3-} and CO_3^{2}) co-doped hydroxyapatite (THA) [$(Ca_{10-\delta}M_{\delta}(PO_4)_{5.5}(CO_3)_{0.5}(OH)_2$, M = trace elements)] integrated with biocompatible magnetic Mn–Zn nanoferrite ((Mn, Zn)Fe_2O_4) nanoparticles (THAiBioMags) on vertebrate development. We found that THAiBioMags, at the concentrations tested, were safe for developing zebrafish embryos. These findings may indicate that there was a strong possibility that THAiBioMags could also be biocompatible in humans.

4 Conclusion

In summary, we successfully developed a multifunctional therapeutic platform (THA) ($Ca_{10-\delta}M_{\delta}(PO_4)_{5.5}(CO_3)_{0.5}(OH)_2$, M = trace elements) by co-doping hydroxyapatite (HA) with multiple trace elements (Mg, Fe, Zn, Mn, Cu, Ni, Mo, Sr, BO_3^{3-} and CO_3^{2-}). This platform allows for the simultaneous loading of magnetic nanoferrite particles (Mn, Zn)Fe_2O_4, (BioMags) and the chemotherapeutic drug (DOX). This innovative approach enables synergistic simultaneous cancer treatment and bone regeneration through precise hyperthermia therapy and localized controlled-release chemotherapy. The physical properties of the as-prepared THAiBioMags particles are distinct from those of the sHA (control), primarily due to their intrinsic magnetic property. These characteristics are significantly influenced by the ion-doping process during synthesis, including the incorporation of (Mn, Zn)Fe_2O_4 nanoferrite into the THA matrix. The synthesized THAiBioMags composite nanoparticles exhibit superparamagnetism with a magnetic saturation of 1.62 emu g^{-1}. Importantly, in the absence of a magnetic field, these synthesized nanoparticles demonstrate minimal or no cytotoxic effects on cell lines. The cytotoxicity assay study demonstrated that the hyperthermia treatment, which raised the temperature to around 45 °C, induced cell death in cancer cells. The synthesized nanoparticles exhibited excellent heating efficiency as a nanoheater, with a specific absorption rate (SAR) value of 9.44 W g^{-1} when subjected to an alternating magnetic field. The THAiBioMags were loaded with DOX and presented sustained drug release at a neutral medium. The DOX release kinetic profile was best fitted with the Weibull model, in which the obtained parameters ("n" was 0.34 and "b" was 0.7) indicated a Fickian release for THAiBioMags. In biological studies, none of the substrates exhibit a cytotoxic effect on rat osteoblast-like UMR-106 cells. Furthermore, the UMR-106 cells showed good adhesion with better dispersion and better viability on the surface of the THAiBioMags substrates. Zebrafish embryo experiments further confirmed the non-toxicity of the THAiBioMags composite particles at the concentration range of 0–500 μg L^{-1}. This research offers valuable insights into the design of a magnetic scaffold with multifunctional properties as a promising candidate for future development into bone scaffolds for therapeutic and bone regeneration purposes.

Data availability

The data that support the findings of this study are available upon request from the authors.

Author contributions

Tanatsaparn Tithito: materials synthesis, investigation, data analysis and writing – original draft; Siwapech Sillapaprayoon:

methodology, investigation; Varissara Chantho: methodology, investigation; Wittaya Pimtong: methodology, investigation, writing – review & editing; Jirawan Thongbunchoo: methodology, investigation; Narattaphol Charoenphandhu: conceptualization, data analysis, criticism, writing – review & editing, supervision, research design, conclusion; Nateetip Krishnamra: data analysis, criticism, writing – review & editing; Nararat Yong: methodology, investigation; Aurachat Lert-itthiporn: methodology, investigation; Weerakanya Maneeprakorn: conceptualization, formal analysis, writing – review & editing, resources; Weeraphat Pon-On: conceptualization, formal analysis, resources, writing – review & editing, supervision, funding acquisition.

Conflicts of interest

There are no conflicts to declare.

Acknowledgements

The authors would like to acknowledge the National Research Council of Thailand (NRCT)-Kasetsart University (NRCTS-RSA63002-03, to W. P.) and support by NSRF *via* the Program Management Unit for Human Resources & Institutional Development, Research and Innovation [grant number B05F640161] (to W. P.). N. Charoenphandhu was supported by Mahidol University [Fundamental Fund: fiscal year 2023 and 2024 by National Science Research and Innovation Fund (NSRF)], the National Research Council of Thailand–Mahidol University Grant (Distinguished Research Professor Grant), and the Faculty of Science, Mahidol University (CIF and CNI grant to N. Charoenphandhu and Research Assistant Grant to N. Charoenphandhu and J. Thongbunchoo). W. Maneeprakorn was supported by Thailand Science Research and Innovation (TSRI) *via* Program Management Unit on Area Based Development (PMUA) and Agricultural Research Development Agency (Public Organization) of Thailand (ARDA).

References

1 B. Chen, H. Xiang, S. Pan, L. Yu, T. Xu and Y. Chen, Advanced Theragenerative Biomaterials with Therapeutic and Regeneration Multifunctionality, *Adv. Funct. Mater.*, 2020, **30**(34), 2002621.

2 H. Wei, J. Cui, K. Lin, J. Xie and X. Wang, Recent advances in smart stimuli-responsive biomaterials for bone therapeutics and regeneration, *Bone Res.*, 2022, **10**, 17.

3 J. Yuan, Z. Ye, Y. Zeng, Z. Pan, Z. Z. Feng, Y. Bao, Y. Li, X. Liu, Y. He and Q. Feng, Bifunctional scaffolds for tumor therapy and bone regeneration: Synergistic effect and interplay between therapeutic agents and scaffold materials, *Mater. Today Bio*, 2022, **15**, 100318.

4 T. M. Oliveira, F. C. Brandão Berti, S. C. Gasoto Jr, B. Schneider, M. A. Stimamiglio and L. F. Berti, Calcium Phosphate-Based Bioceramics in the Treatment of Osteosarcoma: Drug Delivery Composites and Magnetic Hyperthermia Agents, *Front. Med. Technol.*, 2021, **3**, 700266.

5 S. Mondal, P. Manivasagan, S. Bharathiraja, M. S. Moorthy, H. H. Kim, H. Seo, K. D. Lee and J. Oh, Magnetic hydroxyapatite: a promising multifunctional platform for nanomedicine application, *Int. J. Nanomed.*, 2017, **12**, 8389–8410.

6 Y. Xia, H. Chen, Y. Zhao, F. Zhang, X. Li, L. Wang, M. D. Weir, J. Ma, M. A. Reynolds, N. Gu and H. H. K. Xu, Novel magnetic calcium phosphate-stem cell construct with magnetic field enhances osteogenic differentiation and bone tissue engineering, *Mater. Sci. Eng., C*, 2019, **98**, 30–41.

7 J. A. Ramos-Guivar, M. A. Morales and F. J. Litterst, γ-Fe_2O_3 nanoparticles embedded in nanohydroxyapatite matrix for magnetic hyperthermia and *in vitro* osteoblast cell studies, *Ceram. Interfaces*, 2020, **46**, 10658–10666.

8 X. Sun, Y. Gao, Z. Li, J. He and Y. Wu, Magnetic responsive hydroxyapatite scaffold modulated macrophage polarization through PPAR/JAK-STAT signaling and enhanced fatty acid metabolism, *Biomaterials*, 2023, **295**, 122051.

9 K. Marycz, A. Śmieszek, K. Kornicka-Garbowska, A. Pielok, M. Janeczek, A. Lipińska, A. Nikodem, J. Filipiak, P. Sobierajska, J. M. Nedelec and R. J. Wiglusz, Novel Nanohydroxyapatite (nHAp)-Based Scaffold Doped with Iron Oxide Nanoparticles (IO), Functionalized with Small Non-Coding RNA (miR-21/124) Modulates Expression of Runt-Related Transcriptional Factor 2 and Osteopontin, Promoting Regeneration of Osteoporotic Bone in Bilateral Cranial Defects in a Senescence-Accelerated Mouse Model (SAM/P6). PART 2, *Int. J. Nanomed.*, 2021, **16**, 6049–6065.

10 S. Mondal, P. Manivasagan, S. Bharathiraja, M. S. Moorthy, Z. T. Nguyen, H. H. Kim, S. Y. Nam, K. D. Lee and J. Oh, Hydroxyapatite Coated Iron Oxide Nanoparticles: A Promising Nanomaterial for Magnetic Hyperthermia Cancer Treatment, *Nanomaterials*, 2017, **7**, 426.

11 T. S. S. Carvalho, P. M. C. Torres, J. H. Belo, J. Mano and S. M. Olhero, Bioactive Magnetic Materials in Bone Tissue Engineering: A Review of Recent Findings in CaP-Based Particles and 3D-Printed Scaffolds, *Adv. NanoBiomed Res.*, 2023, **3**(9), 2300035.

12 B. Srinivasan, E. Kolanthai, N. E. A. Kumaraswamy, R. R. Jayapalan, D. S. Vavilapalli, L. H. Catalani, G. S. Ningombam, N. S. Khundrakpam, N. R. Singh and S. N. Kalkura, Thermally Modified Iron-Inserted Calcium Phosphate for Magnetic Hyperthermia in an Acceptable Alternating Magnetic Field, *J. Phys. Chem. B*, 2019, **123**, 5506–5513.

13 S. Y. Park, S. K. M. Perikamana, J. H. Park, S. W. Kim, H. Shin, S. P. Park and H. S. Jung, Osteoinductive Superparamagnetic Fe nanocrystal/Calcium Phosphate Heterostructured Microspheres, *Nanoscale*, 2017, **9**, 19145–19153.

14 M. Miola, Y. Pakzad, S. Banijamali, S. Kargozar, C. Vitale-Brovarone, A. Yazdanpanah, O. Bretcanu, A. Ramedani, E. Vernè and M. Mozafari, Glass-ceramics for cancer treatment: So close, or yet so far?, *Acta Biomater.*, 2019, **83**, 55–70.

15 S. S. Danewalia and K. Singh, Bioactive glasses and glass-ceramics for hyperthermia treatment of cancer: state-of-art, challenges, and future perspectives, *Mater. Today Bio*, 2021, **10**, 100100.

16 R. Borges, L. Mendonça-Ferreira, C. Rettori, I. S. O. Pereira, F. Baino and J. Marchi, New sol-gel-derived magnetic bioactive glass-ceramics containing superparamagnetic hematite nanocrystals for hyperthermia application, *Mater. Sci. Eng., C*, 2021, **120**, 111692.

17 R. Borges, L. M. Ferreira, C. Rettori, I. M. Lourenço, A. B. Seabra, F. A. Müller, E. P. Ferraz, M. M. Marques, M. Miola, F. Baino, J. B. Mamani, L. F. Gamarra and J. Marchi, Superparamagnetic and highly bioactive SPIONS/bioactive glass nanocomposite and its potential application in magnetic hyperthermia, *Biomater. Adv.*, 2022, **135**, 112655.

18 Q. Lei, Y. Chen, S. Gao, J. Li, L. Xiao, H. Huang, Q. Zhang, T. Zhang, F. Yan and L. Cai, Enhanced magnetothermal effect of high porous bioglass for both bone repair and antitumor therapy, *Mater. Des.*, 2023, **227**, 111754.

19 Z. Zhang, N. Zhang, X. Li, G. Li, K. Zhang, A. Jing, J. Li and H. Tang, Porous magnetic Fe_3O_4/bioactive glass-ceramic (CaO-SiO_2-P_2O_5-MgO) scaffold with enhanced self-heating ability for hyperthermia treatment of bone tumor-an *in vitro* study, *J. Aust. Ceram. Soc.*, 2022, **58**, 1729–1745.

20 C. Taşar and B. Ercan, Fabrication and biological properties of magnetic bioactive glass nanoparticles, *Ceram. Interfaces*, 2023, **49**(8), 12925–12933.

21 J. Gu, X. Liu, P. Cui and X. Yi, Multifunctional bioactive glasses with spontaneous degradation for simultaneous osteosarcoma therapy and bone regeneration, *Biomater. Adv.*, 2023, **154**, 213626.

22 Nitu, R. Fopase, L. M. Pandey, P. Seal, J. P. Borah and A. Srinivasan, Assessment of sol-gel derived iron oxide substituted 45S5 bioglass-ceramics for biomedical applications, *J. Mater. Chem. B*, 2023, **11**, 7502–7513.

23 A. Ressler, A. Z. Zi, I. Ivanisevi, N. Kamboj and H. Ivankovic, Ionic substituted hydroxyapatite for bone regeneration applications: A review, *Open Ceram.*, 2021, **6**, 100122.

24 E. Bosch-Rué, L. Diez-Tercero, B. Giordano-Kelhoffer, L. M. Delgado, B. M. Bosch, M. Hoyos-Nogués, M. A. Mateos-Timoneda, P. A. Tran, F. J. Gil and R. A. Perez, Biological Roles and Delivery Strategies for Ions to Promote Osteogenic Induction, *Front. Cell Dev. Biol.*, 2021, **8**, 614545.

25 M. Vukomanovic, L. Gazvoda, N. Anicic, M. Rubert, D. Suvorov, R. Müller and S. Hofmann, Multi-doped apatite: Strontium, magnesium, gallium and zinc ions synergistically affect osteogenic stimulation in human mesenchymal cells important for bone tissue engineering, *Biomater. Adv.*, 2022, **140**, 213051.

26 K. Hurle, J. M. Oliveira, R. L. Reis, S. Pina and F. Goetz-Neunhoeffer, Ion-doped Brushite Cements for Bone Regeneration, *Acta Biomater.*, 2021, **123**, 51–71.

27 Q. Yang, L. Jianbo, R. Jie, L. Junzhao, L. Chao and S. Donglu, Enhanced Magnetic Fluid Hyperthermia by Micellar Magnetic Nanoclusters Composed of $Mn_xZn_{1-x}Fe_2O_4$ Nanoparticles for Induced Tumor Cell Apoptosis, *ACS Appl. Mater. Interfaces*, 2014, **6**, 16867–16879.

28 J. Xie, Y. Zhang, C. Yan, L. Song, S. Wen, F. Zang, G. Chen, Q. Ding, C. Yan and N. Gu, High-performance PEGylated Mn–Zn ferrite nanocrystals as a passive-targeted agent for magnetically induced cancer theranostics, *Biomaterials*, 2014, **35**, 9126–9136.

29 J. Xie, C. Yan, Y. Yan, L. Chen, L. Song, F. Zang, Y. An, G. Teng, N. Gu and Y. Zhang, Multi-modal Mn–Zn ferrite nanocrystals for magnetically-induced cancer targeted hyperthermia: a comparison of passive and active targeting effects, *Nanoscale*, 2016, **8**, 16902–16915.

30 N. Jović Orsini, M. M. Milić and T. E. Torres, Zn- and (Mn, Zn)-substituted *versus* unsubstituted magnetite nanoparticles: structural, magnetic and hyperthermic properties, *Nanotechnology*, 2020, **31**, 225707.

31 W. Montha, W. Maneeprakorn, N. Buatong, I. M. Tang and W. Pon-On, Synthesis of doxorubicin-PLGA loaded chitosan stabilized (Mn, Zn)Fe_2O_4 nanoparticles: Biological activity and pH-responsive drug release, *Mater. Sci. Eng., C*, 2016, **59**, 235–240.

32 N. A. Peppas and P. Colombo, Analysis of drug release behavior from swellable polymer carriers using the dimensionality index, *J. Controlled Release*, 1997, **45**, 35–40.

33 N. V. Mdlovu, R. S. Juang, M. T. Weng, Y. S. Lin and K. S. Lin, Dual pH-/Thermoresponsive Shell-Cross-Linked Magnetic Mesoporous Nanospheres for Doxorubicin Delivery and *In Vitro*/*In Vivo* Cancer Treatment, *ACS Appl. Nano Mater.*, 2023, **6**(10), 8416–8433.

34 V. Papadopoulou, K. Kosmidis, M. Vlachou and P. Macheras, On the use of the Weibull function for the discernment of drug release mechanisms, *Int. J. Pharm.*, 2006, **309**, 44–50.

35 A. Das, S. Mohanty, R. Kumar and B. K. Kuanr, Tailoring the Design of a Lanthanide Complex/Magnetic Ferrite Nanocomposite for Efficient Photoluminescence and Magnetic Hyperthermia Performance, *ACS Appl. Mater. Interfaces*, 2020, **12**, 42016–42029.

36 R. R. Wildeboer, P. Southern and Q. A. Pankhurst, On the Reliable Measurement of Specific Absorption Rates and Intrinsic Loss Parameters in Magnetic Hyperthermia Materials, *J. Phys. D: Appl. Phys.*, 2014, **47**, 495003.

37 W. Pon-On, N. Charoenphandhu, J. Teerapornpuntakit, J. Thongbunchoo, N. Krishnamra and I. M. Tang, Mechanical properties, biological activity and protein controlled release by poly(vinyl alcohol)-bioglass/chitosan-collagen composite scaffolds: A bone tissue engineering applications, *Mater. Sci. Eng., C*, 2014, **38**, 63–72.

38 The Organization for Economic Co-operation and Development (OECD), *Test No. 236: Fish Embryo Acute Toxicity (FET) Test, OECD Guidelines for the Testing of Chemicals, Section 2*, OECD Publishing, Paris, 2013, **https://www.oecd-ilibrary.org/environment/test-no-236-fishembryo-acute-toxicity-fet-test_9789264203709-en**.

39 R. Hergt and S. Dutz, Magnetic particle hyperthermia-biophysical limitations of a visionary tumour therapy, *J. Magn. Magn. Mater.*, 2007, **311**, 187–192.

40 X. Liu, Y. Zhang, Y. Wang, W. Zhu, G. Li, X. Ma, Y. Zhang, S. Chen, S. Tiwari, K. Shi, S. Zhang, H. M. Fan, Y. X. Zhao and X. J. Liang, Comprehensive understanding of magnetic hyperthermia for improving antitumor therapeutic efficacy, *Theranostics*, 2020, **10**(8), 3793–3815.

41 E. C. Abenojar, S. Wickramasinghe, J. Bas-Concepcion and A. C. S. Samia, Structural effects on the magnetic hyperthermia properties of iron oxide nanoparticles, *Prog. Nat. Sci.: Mater. Int.*, 2016, **26**, 440–448.

42 I. M. Obaidat, V. Narayanaswamy, S. Alaabed, S. Sambasivam and C. V. V. Muralee Gopi, Principles of Magnetic Hyperthermia: A Focus on Using Multifunctional Hybrid Magnetic Nanoparticles, *Magnetochemistry*, 2019, **5**, 67.

43 E. Myrovali, K. Papadopoulos, G. Charalampous, P. Kesapidou, G. Vourlias, T. Kehagias, M. Angelakeris and U. Wiedwald, Toward the Separation of Different Heating Mechanisms in Magnetic Particle Hyperthermia, *ACS Omega*, 2023, **8**, 12955–12967.

44 V. Pilati, G. Gomide, R. C. Gomes, G. F. Goya and J. Depeyrot, Colloidal Stability and Concentration Effects on Nanoparticle Heat Delivery for Magnetic Fluid Hyperthermia, *Langmuir*, 2021, **37**, 1129–1140.

45 M. S. Ur Rahman, M. A. Tahir, S. Noreen, M. Yasir, I. Ahmad, M. B. Khan, K. W. Ali, M. Shoaib, A. Bahadur and S. Iqbal, Magnetic mesoporous bioactive glass for synergetic use in bone regeneration, hyperthermia treatment, and controlled drug delivery, *RSC Adv.*, 2020, **10**, 21413.

46 A. K. Yadav, H. Tripathi, A. Bastia, P. Singh, A. K. Dubey, N. S. Anuraag, N. K. Prasad and C. Rath, Synergistic effect of $CoFe_2O_4$-85S nano bio-glass composites for hyperthermia and controlled drug delivery, *Materialia*, 2023, **32**, 101884.

47 H. Zhao, C. Liu, Y. Liu, Q. Ding, T. Wang, H. Li, H. Wu and T. Ma, Harnessing electromagnetic fields to assist bone tissue engineering, *Stem Cell Res. Ther.*, 2023, **14**, 7.

48 T. P. Ribeiro, M. Flores, S. Madureira, F. Zanotto, F. J. Monteiro and M. S. Laranjeira, Magnetic Bone Tissue Engineering: Reviewing the Effects of Magnetic Stimulation on Bone Regeneration and Angiogenesis, *Pharmaceutics*, 2023, **15**, 1045.

49 C. Shuai, Y. Cheng, W. Yang, P. Feng, Y. Yang, C. He, F. Qi and S. Peng, Magnetically actuated bone scaffold: Microstructure, cell response and osteogenesis, *Composites, Part B*, 2020, **192**, 107986.

50 S. Pujari-Palmer, X. Lu and M. K. Ott, The Influence of Hydroxyapatite Nanoparticle Morphology on Embryonic Development in a Zebrafish Exposure Model, *Nanomaterials*, 2017, **7**, 89.

51 L. B. Romero-Sánchez, M. Marí-Beffa, P. Carrillo, M. A. Medina and A. Díaz-Cuenca, Copper-containing mesoporous bioactive glass promotes angiogenesis in an *in vivo* zebrafish model, *Acta Biomater.*, 2018, **68**, 272–285.

52 H. Makkar, S. K. Verma, P. K. Panda, E. Jha, B. Das, K. Mukherjee and M. Suar, *In Vivo* Molecular Toxicity Profile of Dental Bioceramics in Embryonic Zebrafish (Danio rerio), *Chem. Res. Toxicol.*, 2018, **31**, 914–923.

53 L. Fua, Y. Xiong, G. Carlssonb, M. Palmer, S. Örn, W. Zhu, X. Weng, H. Engqvist and W. Xi, Biodegradable Si_3N_4 bioceramic sintered with Sr, Mg and Si for spinal fusion: Surface characterization and biological evaluation, *Appl. Mater. Today*, 2018, **12**, 260–275.